Environmental Science & Technology

pubs.acs.org/est

Article

Enhancing the Carbon Monoxide Oxidation Performance through Surface Defect Enrichment of Ceria-Based Supports for Platinum Catalyst

Shaohua Xie, Yue Lu, Kailong Ye, Wei Tan, Sufeng Cao, Chunying Wang, Daekun Kim, Xing Zhang, Jeremia Loukusa, Yaobin Li, Yan Zhang, Lu Ma, Steven N. Ehrlich, Nebojsa S. Marinkovic, Jiguang Deng, Maria Flytzani-Stephanopoulos, and Fudong Liu*

Cite This: *Environ. Sci. Technol.* 2024, 58, 12731−12741

Read Online

ACCESS | Metrics & More | Article Recommendations | Supporting Information

ABSTRACT: Effective synthesis and application of single-atom catalysts on supports lacking enough defects remain a significant challenge in environmental catalysis. Herein, we present a universal defect-enrichment strategy to increase the surface defects of CeO_2-based supports through H_2 reduction pretreatment. The Pt catalysts supported by defective CeO_2-based supports, including CeO_2, $CeZrO_x$, and CeO_2/Al_2O_3 (CA), exhibit much higher Pt dispersion and CO oxidation activity upon reduction activation compared to their counterpart catalysts without defect enrichment. Specifically, Pt is present as embedded single atoms on the CA support with enriched surface defects (CA-HD) based on which the highly active catalyst showing embedded Pt clusters (Pt_C) with the bottom layer of Pt atoms substituting the Ce cations in the CeO_2 surface lattice can be obtained through reduction activation. Embedded Pt_C can better facilitate CO adsorption and promote O_2 activation at Pt_C−CeO_2 interfaces, thereby contributing to the superior low-temperature CO oxidation activity of the Pt/CA-HD catalyst after activation.

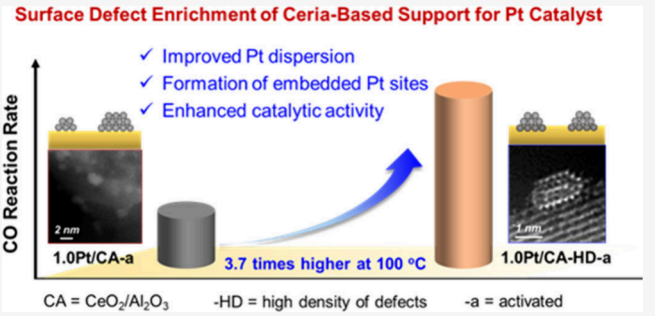

KEYWORDS: *surface defect enrichment, Pt single-atom catalyst, embedded Pt cluster, CO adsorption, O_2 activation*

1. INTRODUCTION

Nowadays, supported metal single-atom catalysts (SACs) have garnered significant attention as a result of their 100% metal utilization efficiency and great benefits in various catalytic reactions, including organic catalysis, photocatalysis, electrocatalysis, and thermal catalysis.[1−6] In environmental catalysis, such as the catalytic oxidation of CO,[7] one of the critical reactions in purifying vehicle emissions, SACs usually exhibit low instinct activity. This is primarily attributed to the lack of synergistic effects from neighboring metal atoms,[8,9] making their direct application highly challenging. In addition to the tuning of local structures of metal sites in SACs,[10−14] reduction activation has been proven to be a facile and effective approach to activate less active SACs into more efficient oxidation catalysts,[8,15] with SACs serving as catalyst precursors. Interestingly, the activated catalysts derived from SACs typically show significantly higher catalytic performance compared to those prepared directly using conventional methods, such as for CO and hydrocarbon oxidation reactions.[15−17] Surface defects of metal oxide supports have been shown to be crucial for anchoring metal atoms,[15,18,19] but the limited concentration of surface defects on regular metal oxides makes them difficult to afford high loading of metal single atoms. Therefore, the development of a universal approach to increase the surface defects of metal oxide supports is highly desired for the preparation of SACs with a high metal loading and superior catalytic activity.

Precious metal catalysts are widely used in automotive exhaust control as a result of their excellent performance.[20,21] However, the high usage amount of precious metals and poor low-temperature performance after long-term operation remain the major challenges in practical applications.[21] In comparison to more expensive Pd and Rh catalysts nowadays, Pt catalysts have recently attracted huge interest, owing to their favorable cost-effectiveness and superior catalytic performance. In particular, Pt/CeO_2-based catalysts have been extensively investigated and show high potential in vehicle exhaust treatment systems.[10,22] To further improve their catalytic activity and thermal stability, the preparation of CeO_2 supports

Received: March 27, 2024
Accepted: June 18, 2024
Published: July 3, 2024

https://doi.org/10.1021/acs.est.4c03078
Environ. Sci. Technol. 2024, 58, 12731−12741

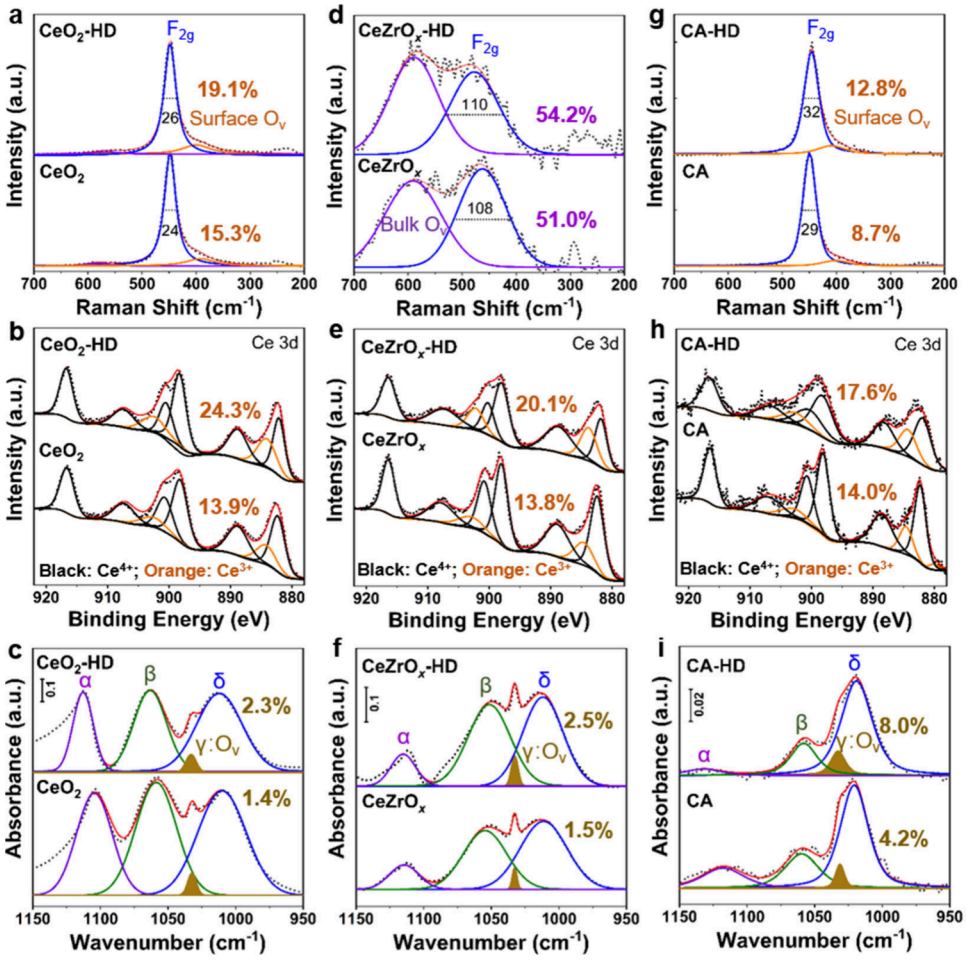

Figure 1. Characterizations of surface defects: (a, d, and g) Raman spectra, (b, e, and h) Ce 3d XPS, and (c, f, and i) *in situ* DRIFTS of methanol adsorption at 25 °C on (a−c) CeO_2, (d−f) $CeZrO_x$, and (g−i) CA with and without H_2 reduction. The $O_v/(O_{latt} + O_v)$ ratios, $Ce^{3+}/(Ce^{3+} + Ce^{4+})$ ratios, and surface O_v concentrations are inserted in related figures.

with abundant surface defects as Pt anchoring sites can be a promising approach.[19] Traditional methods for increasing the surface defects of CeO_2 involve the usage of dopants as structure modifiers or the controllable preparation of CeO_2 with specific exposed crystal planes.[23−25] However, these methods usually require expensive raw materials (*e.g.*, La, Y, Pr, Nd, Sm, *etc.*) or complex preparation procedures (such as hydrothermal synthesis and precipitation method),[26−29] limiting their wide applications.

Reducible metal oxides, which have lattice oxygen that can be easily removed by reduction treatment using reductive gases, such as H_2, at specific temperatures, show great potential for enriching the surface defects and serving as effective supports for SACs with increased metal loading. In this study, we demonstrate a general H_2 reduction strategy for enriching the surface defects of CeO_2-based oxide supports, including pure CeO_2, $CeZrO_x$, and CeO_2/Al_2O_3 (CA). It has been demonstrated that the Pt catalysts on the defect-enriched CeO_2-based supports exhibit much higher Pt dispersion and CO oxidation activity upon reduction activation compared to their counterparts without surface defect enrichment. For example, when 1 wt % Pt catalysts on CA supports are taken as examples, the Pt microstructures within the catalysts before and after reduction activation are systematically investigated using multiple techniques, including *in situ* diffuse reflectance infrared Fourier transform spectroscopy (*in situ* DRIFTS), scanning transmission electron microscopy (STEM), extended X-ray absorption fine structure (EXAFS), *etc.* Along with kinetics and *in situ* X-ray absorption spectroscopy (XAS) studies, the structure−activity relationship for CO oxidation on these Pt/CA catalysts has been clearly revealed. On the defect-enriched CA support (CA-HD, where -HD is the high density of defects), a unique Pt cluster (Pt_C) site can be fabricated, where the bottom layer of Pt atoms embedded in the CeO_2 surface matrix. Such a unique Pt_C site originated from the reduction activation of Pt single atoms (Pt_1) on CA-HD, which can effectively facilitate the CO adsorption and O_2 activation at Pt_C-CeO_2 interfaces, resulting in superior activity in low-temperature CO oxidation.

2. MATERIALS AND METHODS

2.1. Catalyst Preparation. *2.1.1. Preparation of Ceria-Based Supports with/without Defect Enrichment.* Commercial CeO_2 [Brunauer−Emmett−Teller (BET) surface area of 120 m^2/g, Solvay], commercial $CeZrO_x$ (40 wt % CeO_2, Solvay), and CeO_2/Al_2O_3 (30 wt % CeO_2) supports were used in this work for defect enrichment and subsequent Pt loading. The CeO_2/Al_2O_3 support was prepared using a conventional incipient wetness impregnation (IWI) method. Typically, a solution of $Ce(NO_3)_3{\cdot}6H_2O$ (99.5%, Acros Organics) with a predetermined concentration was added dropwise onto γ-Al_2O_3 (BET surface area of 150 m^2/g, Sasol) under stirring.

https://doi.org/10.1021/acs.est.4c03078
Environ. Sci. Technol. 2024, 58, 12731−12741

The CeO_2/Al_2O_3 support was obtained by subsequent calcination in air at 550 °C for 2 h. To enrich surface defects on CeO_2, $CeZrO_x$, and CeO_2/Al_2O_3 supports, the supports were reduced in 10% H_2/Ar flow at 750 °C for 2 h with a temperature ramping rate of 5 °C/min. These supports with defect enrichment are denoted as CeO_2-HD, $CeZrO_x$-HD, and CA-HD, respectively. For direct comparison, regular CeO_2, $CeZrO_x$, and CeO_2/Al_2O_3 (denoted as CA) were further calcined in air at 750 °C for 2 h with the temperature ramping rate of 5 °C/min.

2.1.2. Preparation of Pt Catalysts. The catalysts with 1 wt % of Pt loading on CeO_2, CeO_2-HD, $CeZrO_x$, and $CeZrO_x$-HD supports were prepared using the IWI method and tetraammineplatinum nitrate (TAPN) as the precursor. The TAPN solution with a predetermined concentration was added dropwise onto the supports under stirring and then dried at 120 °C for 1 h. After calcination in air at 550 °C for 2 h with a temperature ramping rate of 5 °C/min, the catalysts were obtained and denoted as Pt/CeO_2, Pt/CeO_2-HD, $Pt/CeZrO_x$, and $Pt/CeZrO_x$-HD, respectively. The catalysts with x wt % of Pt loadings (x = 0.5, 1.0, and 5.0) on CA, CA-HD, and pristine γ-Al_2O_3 supports were prepared using IWI method as well with TAPN as the precursor. The obtained catalysts with different Pt loadings were denoted as xPt/CA, xPt/CA-HD, and xPt/Al_2O_3, respectively. To study the effects of reduction activation on CO oxidation activity, all catalysts were reduced in 10% H_2 flow at 400 °C for 1 h with the temperature ramping rate of 10 °C/min and labeled with "-a" (where -a is activated).

2.2. Catalyst Characterizations. The detailed descriptions of catalyst characterizations by X-ray diffraction (XRD), Raman spectroscopy, STEM, *in situ* DRIFTS, X-ray photoelectron spectroscopy (XPS), XAS, H_2 temperature-programmed reduction (H_2-TPR), and dynamic oxygen storage capacity (OSC) techniques can be found in the Supporting Information

2.3. Catalytic Performance Evaluation. The CO oxidation reaction was conducted in a flow-through fixed bed quartz tubular reactor (inner diameter = 4 mm) system. In each test, 25 mg of catalyst (40−60 mesh) was diluted with inert SiC powder (0.25 g) to prevent temperature gradients. The steady-state CO oxidation activity was measured with a duration time of 30 min at each temperature point. The feeding stream consisted of 1% CO and 1% O_2 balanced with Ar. The total flow rate was fixed at 83.33 mL/min, achieving a weight hourly space velocity (WHSV) of 200 000 $mL \cdot g^{-1} \cdot h^{-1}$. A catalytic stability test of 1.0Pt/CA-a and 1.0Pt/CA-HD-a catalysts was performed at 100 °C with or without 5% H_2O in the feedstock at a WHSV of 300 000 $mL \cdot g^{-1} \cdot h^{-1}$. The reactants and products were analyzed online by mass spectrometry (MS, HPR-20 R&D, Hiden Analytical) using the m/z ratios of 28, 32, and 44 used for monitoring CO, O_2, and CO_2, respectively. To avoid significant heat or mass transfer limitation, the kinetic study was performed with CO conversion below 16% under a WHSV of 500 000 $mL \cdot g^{-1} \cdot h^{-1}$.

3. RESULTS AND DISCUSSION

3.1. Effects of Reduction on Enriching the Surface Defects of CeO_2-Based Supports. The formation of additional defects on CeO_2-based supports as a result of H_2 reduction was clearly evidenced by Raman spectra, Ce 3d XPS, and *in situ* DRIFTS of methanol adsorption (at 25 °C). When pure CeO_2 was taken as an example, as shown in Figure 1a, two characteristic peaks located at 448 and 400 cm^{-1} were observed in Raman spectra, which can be assigned to the typical vibration mode (F_{2g}) of the fluorite-type CeO_2 structure and the near-surface oxygen vacancies (O_v),[30,31] respectively. In comparison to CeO_2, reduced CeO_2-HD exhibited a much higher $O_v/(O_{latt} + O_v)$ ratio (19.1% for CeO_2-HD versus 15.3% for CeO_2, where O_{latt} is lattice oxygen) and a broader half-width of the F_{2g} peak (26 cm^{-1} for CeO_2-HD versus 24 cm^{-1} for CeO_2), suggesting a significant increase in the density of defects (mainly O_v) and a decrease in the crystallinity of CeO_2-HD.[31] The increase in defect density was further confirmed by Ce 3d XPS and *in situ* DRIFTS of the methanol adsorption results. As depicted in Figure 1b, both surface Ce^{3+} and Ce^{4+} species were observed on CeO_2 and CeO_2-HD supports.[12,32] Notably, CeO_2-HD exhibited a significantly higher concentration of surface Ce^{3+} species (24.3%) compared to CeO_2 (13.9%). Upon methanol adsorption, four types of methoxy species were identified on both CeO_2 and CeO_2-HD (Figure 1c), including linearly adsorbed methoxy species (peak α), bridgingly adsorbed methoxy species on Ce^{4+} cations without O_v (peak β) and with O_v (peak γ) in the neighborhood, and three-coordinated methoxy species (peak δ),[33] respectively. It was clearly observed that more methoxy species adsorbed on Ce^{4+} cations with O_v nearby were present on CeO_2-HD than on CeO_2 (2.3% for CeO_2-HD versus 1.4% for CeO_2). Such an effect of H_2 reduction on enriching the surface defects was also observed on $CeZrO_x$ and CA supports. As shown in panels d−i of Figure 1, after H_2 reduction, the half-widths of the F_{2g} peak and the $O_v/(O_{latt} + O_v)$ ratios observed in Raman spectra, the $Ce^{3+}/(Ce^{3+} + Ce^{4+})$ ratios determined by Ce 3d XPS, and the surface O_v concentrations measured by methanol adsorption on $CeZrO_x$-HD and CA-HD supports were broader or much higher than those on their counterparts without defect enrichment ($CeZrO_x$ and CA), respectively. It should be noticed that, different from O_v observed on CeO_2 and CA supports (panels a and g of Figure 1), the bulk O_v defects (589 cm^{-1}) nearby Ce^{3+} species were obviously observed on $CeZrO_x$ supports (Figure 1d), which was mainly due to the formation of $CeZrO_x$ solid solution.[30] These results unambiguously indicate that H_2 reduction is a universally effective method to enhance the surface defects on CeO_2-based supports, thereby enabling their application as highly efficient supports for enhancing metal dispersion upon loading.

3.2. Impact of Defect Enrichment on CO Oxidation Activity. To determine if the supports with enriched defects were beneficial for obtaining highly active metal catalysts, the Pt catalysts supported on CeO_2, $CeZrO_x$, and CA with and without defect enrichment were prepared and tested for CO oxidation. As depicted in panels a−d of Figure S1 of the Supporting Information, upon Pt loading, a much brighter color of Pt/CeO_2-HD than that of Pt/CeO_2 was observed, suggesting a higher Pt dispersion achieved on CeO_2-HD than on regular CeO_2. As shown in Figure S1e of the Supporting Information, the as-prepared Pt/CeO_2 catalyst showed higher CO oxidation activity than the Pt/CeO_2-HD catalyst, with a lower T50 (the temperature corresponding to 50% of CO conversion) achieved on the former (188 °C) than on the latter (266 °C). It has been reported that the reduction activation is highly crucial for Pt-CeO_2-based catalysts to achieve excellent catalytic activity for CO oxidation, because it can help generate more active Pt_C species on CeO_2.[16] After H_2 reduction activation in 10% H_2/Ar at 400 °C for 1 h, the light-off curves for CO oxidation on Pt/CeO_2-a and Pt/CeO_2-HD-a

https://doi.org/10.1021/acs.est.4c03078
Environ. Sci. Technol. 2024, 58, 12731−12741

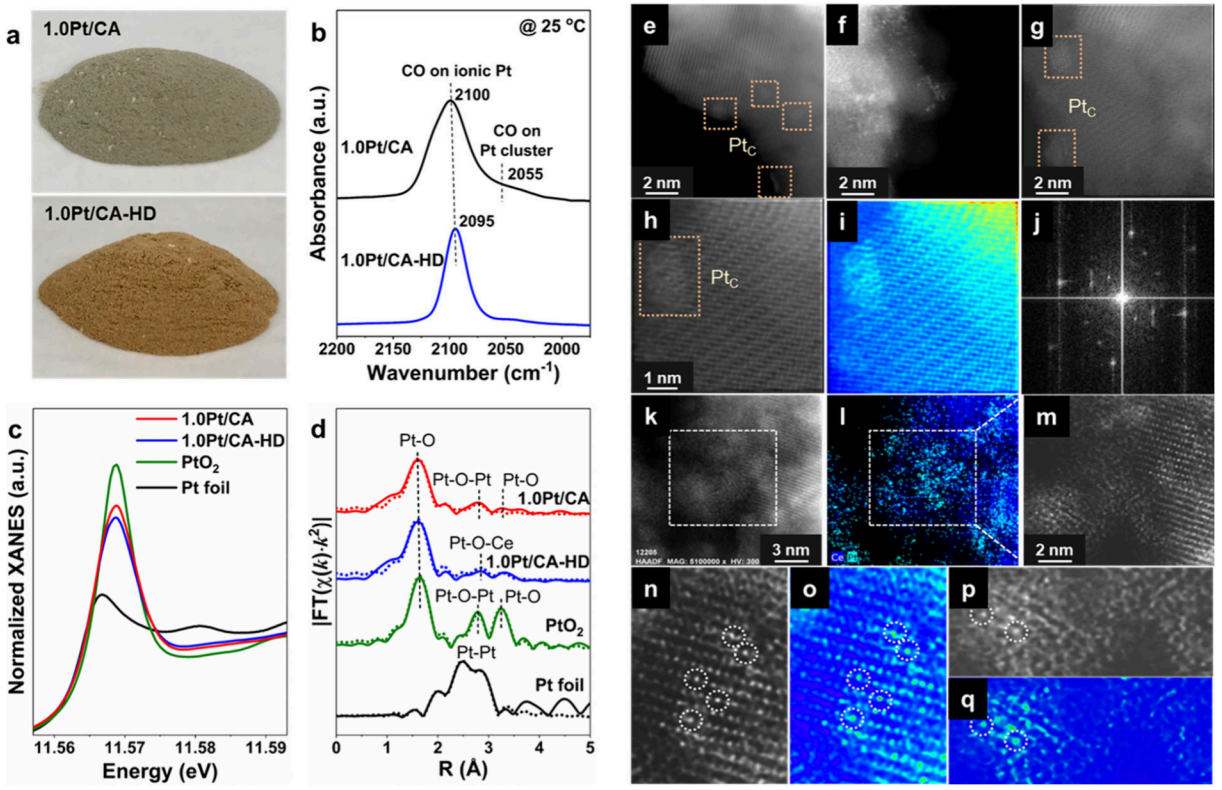

Figure 2. Structure characterizations: (a) photos, (b) *in situ* DRIFTS of CO adsorption, (c) Pt L_3-edge XANES, (d) Pt L_3-edge EXAFS, and (e−q) AC-STEM images for (e−j) 1.0Pt/CA and (k−q) 1.0Pt/CA-HD catalysts.

catalysts (where -a is activated) significantly shifted to a lower temperature range, with a much lower T50 achieved on Pt/CeO_2-HD-a (85 °C) than on Pt/CeO_2-a (108 °C). These results clearly show that the defect enrichment of the pure CeO_2 support greatly improved the dispersion of loaded Pt species and significantly enhanced the CO oxidation performance upon reduction activation. Similarly, the activated Pt catalysts on defect-enriched $CeZrO_x$-HD also showed higher CO oxidation activity than that on $CeZrO_x$ (Figure S2 of the Supporting Information). Such results demonstrate that the defect enrichment strategy for CeO_2-based supports by H_2 reduction is universal for improving the low-temperature CO oxidation activity of supported Pt catalysts after activation and is worthy of systematic investigation, especially for the widely used CA support in industry. Accordingly, the CO oxidation activity of *x*Pt/CA, *x*Pt/CA-HD, and *x*Pt/Al_2O_3 (*x* = 0.5, 1.0, and 5.0 wt %) before and after H_2 reduction activation was investigated (Figure S3 of the Supporting Information). Not surprisingly, the as-prepared *x*Pt/CA catalysts always showed higher CO oxidation activity than *x*Pt/CA-HD and *x*Pt/Al_2O_3 at the same level of Pt loading, mainly as a result of the presence of more active Pt_C species on CeO_2 within *x*Pt/CA catalysts, as confirmed in the subsequent sections. Upon activation, significant enhancement of CO oxidation activity was observed on both *x*Pt/CA-a and *x*Pt/CA-HD-a catalysts in comparison to the less pronounced or no activity promotion on *x*Pt/Al_2O_3. Interestingly, the defect-enriched *x*Pt/CA-HD-a catalysts constantly performed much higher CO oxidation activity than *x*Pt/CA-a and *x*Pt/Al_2O_3-a at the same Pt loading level. Even with the Pt loading as high as 5.0 wt %, the benefit of the support defect enrichment for improving the CO oxidation performance still obviously existed.

3.3. Impact of Defect Enrichment on the Pt Local Structures. The dispersion of precious metals is inherently linked to the density of surface defects on the supports. It was expected that CA-HD with a higher concentration of surface defects could be able to anchor more Pt_1 than CA. To understand the Pt structures in detail, *in situ* DRIFTS of CO adsorption, X-ray absorption near edge structure (XANES), EXAFS, and aberration corrected scanning transmission electron microscopy (AC-STEM) measurements were conducted for 1.0Pt/CA and 1.0Pt/CA-HD. Similar to the observations for Pt/CeO_2-HD and Pt/$CeZrO_x$-HD catalysts, which showed brighter color than Pt/CeO_2 and Pt/$CeZrO_x$ counterpart catalysts, respectively, as a result of higher Pt dispersion benefiting from defect enrichment, the 1.0Pt/CA-HD catalyst also displayed brighter golden color compared to 1.0Pt/CA, which showed a gray greenish color (Figure 2a). *In situ* DRIFTS of CO adsorption (Figure 2b) clearly revealed that only Pt_1 (with CO@Pt_1 at 2095 cm^{-1}) was present on 1.0Pt/CA-HD, while both Pt_1 sites (with CO@Pt_1 at 2100 cm^{-1}) and Pt_C sites (with CO@Pt_C at 2055 cm^{-1}) were present on 1.0Pt/CA.[8,34] The Pt L_3-edge XANES results showed that the Pt species within 1.0Pt/CA and 1.0Pt/CA-HD were both in oxidized states (Figure 2c), which were between Pt^0 and Pt^{4+} but closer to Pt^{4+} based on the white line intensity. As evidenced by the XANES linear combination fitting results (Figure S4 and Table S1 of the Supporting Information), a lower average oxidation state of Pt species was present on 1.0Pt/CA-HD (+2.8) compared to 1.0Pt/CA (+3.1), which was mainly due to the presence of more interaction between $Pt^{4+} + 2Ce^{3+} \rightarrow Pt^{2+} + 2Ce^{4+}$ on 1.0Pt/CA-HD.[14] The EXAFS results in R space (Figure 2d) showed the presence of the Pt−O bond (first shell) and Pt−O−Pt and Pt−O bonds (second

https://doi.org/10.1021/acs.est.4c03078
Environ. Sci. Technol. 2024, 58, 12731−12741

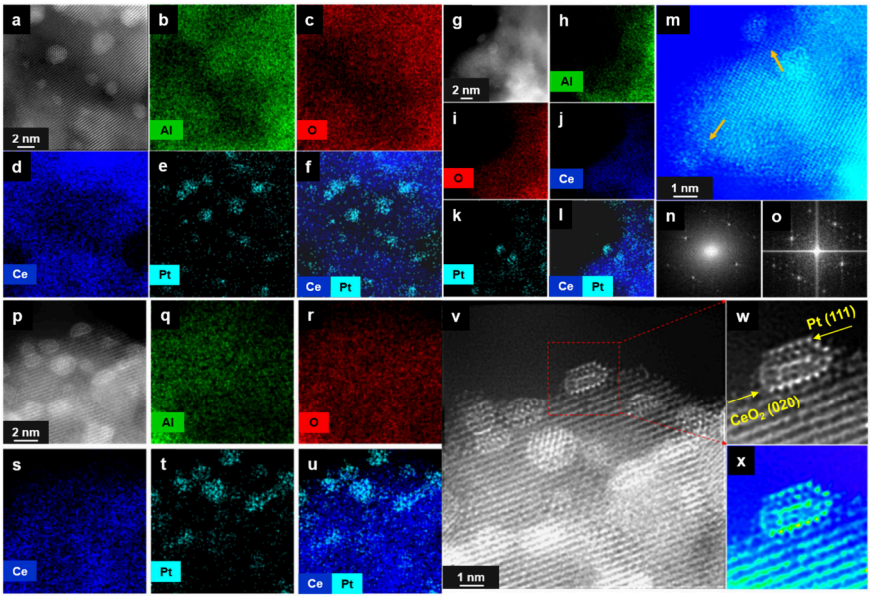

Figure 3. AC-STEM and EDS mapping images for (a−o) 1.0Pt/CA-a and (p−x) 1.0Pt/CA-HD-a catalysts.

shell) in 1.0Pt/CA. In contrast, only Pt−O bonds (first shell) and Pt−O−Ce bonds (second shell) were observed on 1.0Pt/CA-HD. This is notable because the Pt−O−Pt bond appears slightly shorter compared to Pt−O−Ce bonds in phase-uncorrected EXAFS,[35,36] although the length of the latter also depends upon the local structure of Pt on CeO_2. These results suggest the presence of Pt_C species within 1.0Pt/CA and exclusive Pt_1 species within 1.0Pt/CA-HD. The EXAFS curve-fitting results (Table S2 of the Supporting Information) confirmed that the Pt species in 1.0Pt/CA-HD showed a slightly lower coordination number (CN) of Pt−O (4.6) than that in 1.0Pt/CA (4.8), which was in accordance with the Pt oxidation state sequence within the two catalysts. Such Pt L_3-edge XANES and EXAFS results overall suggested that a much stronger interaction between Pt and CeO_2 was present in 1.0Pt/CA-HD than in regular 1.0Pt/CA.

Figure S5 of the Supporting Information shows the energy-dispersive X-ray spectroscopy (EDS) mapping images for the 1.0Pt/CA and 1.0Pt/CA-HD catalysts. A highly consistent distribution of Pt and Ce was observed on both catalysts, suggesting that CeO_2 was beneficial for anchoring the Pt species rather than Al_2O_3. This finding was further supported by the AC-STEM images (panels e−q of Figure 2), which clearly showed both Pt_1 (Figure 2f) and Pt_C (panels g−i of Figure 2) on CeO_2 within 1.0Pt/CA, whereas only Pt_1 (panels n−q of Figure 2) was observed on CeO_2 within 1.0Pt/CA-HD, with Pt_1 substituting Ce sites in the CeO_2 lattice matrix. As expected, the defect enrichment strategy via prer-eduction resulted in a significant benefit in enhancing the dispersion of Pt on CeO_2-based supports. Afterward, the H_2-TPR technique was used to evaluate the reducibility of 1.0Pt/CA and 1.0Pt/CA-HD catalysts with totally distinct Pt species and local structures. As depicted in Figure S6 of the Supporting Information, for both catalysts, three H_2 consumption peaks attributed to the reduction of surface-adsorbed oxygen species (O_{ads}) (85 or 100 °C), Pt−O species (130 or 141 °C), and Pt−O−Ce species (200 or 205 °C) could be observed. In comparison to 1.0Pt/CA, higher reduction temperatures and a larger total H_2 consumption amount were observed for 1.0Pt/CA-HD (268 μmol/g for 1.0Pt/CA-HD versus 123 μmol/g for 1.0Pt/CA below 300 °C), suggesting the much stronger interaction between Pt and CeO_2 in the 1.0Pt/CA-HD catalyst as a result of the presence of more Pt−O−Ce linkages, as evidenced by the EXAFS results.

The Pt structures in the reduction-activated catalysts, including 1.0Pt/CA-a and 1.0Pt/CA-HD-a, were also systematically characterized using *in situ* DRIFTS, XAS, and AC-STEM techniques. As shown in Figure S7a of the Supporting Information, upon H_2 reduction activation and CO adsorption, similar and broad infrared (IR) bands consisting of several subpeaks showed up on both 1.0Pt/CA-a and 1.0Pt/CA-HD-a catalysts. The IR peaks at 2087, 2069, and 2045 cm^{-1} were attributed to the CO linearly adsorbed on terrace sites, step sites, and corner sites (under-coordinated Pt) of formed Pt_C, respectively.[16,37,38] The similar CO adsorption behavior observed on 1.0Pt/CA-a and 1.0Pt/CA-HD-a probably suggested a comparable Pt_C average size within both catalysts.[39] As observed from Pt L_3-edge XANES results (Figures S7b and S4 and Table S1 of the Supporting Information), the reduction activation resulted in a significant decline in the oxidation states of Pt species within 1.0Pt/CA-a (1.5) and 1.0Pt/CA-HD-a (1.7), with the latter catalyst showing a slightly higher Pt oxidation state. This decline was mainly due to the formation of Pt−PtO_x clusters with mixed oxidation states between Pt metal and Pt oxide, as verified by the Pt L_3-edge EXAFS results (Figure S7c and Table S2 of the Supporting Information). These results clearly showed the presence of Pt−Pt bonds (2.63−2.69 Å) from the Pt metallic phase and Pt−O bonds (2.00 Å) from the PtO_x phase within 1.0Pt/CA-a and 1.0Pt/CA-HD-a. The varied Pt−Pt bonds suggest distinct Pt structures within the catalysts. In addition, the higher CN of the Pt−O bond (3.5 versus 2.5) and lower CN of the Pt−Pt bond (2.2 versus 4.3) in 1.0Pt/CA-HD-a compared to that in 1.0Pt/CA-a well elucidated the higher average oxidation state of Pt observed on 1.0Pt/CA-HD-a (1.7 versus 1.5). These phenomena could be attributed to either the formation of smaller Pt−PtO_x clusters or the presence of a stronger interaction between Pt species and CeO_2 within 1.0Pt/CA-HD-a compared to 1.0Pt/CA-a. Further clarification can be obtained by the following AC-STEM analysis.

https://doi.org/10.1021/acs.est.4c03078
Environ. Sci. Technol. 2024, 58, 12731−12741

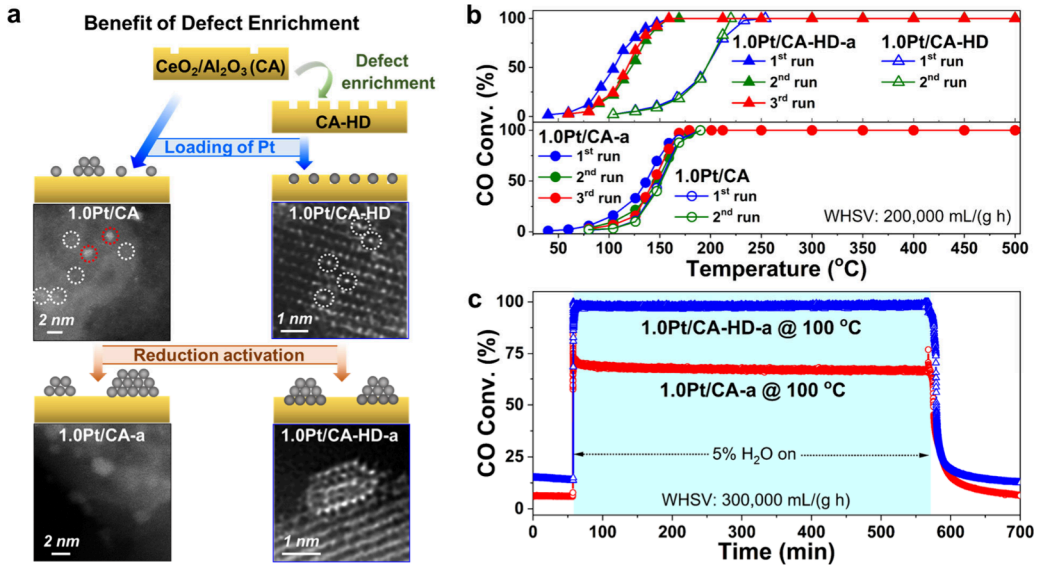

Figure 4. Effect of defect enrichment on CO oxidation activity: (a) scheme for the benefit of defect enrichment and AC-STEM images of 1.0Pt/CA, 1.0Pt/CA-HD, 1.0Pt/CA-a, and 1.0Pt/CA-HD-a catalysts and CO oxidation activity on 1.0Pt/CA-a and 1.0Pt/CA-HD-a catalysts (b) during the cycling test (from 40 to 500 °C) and (c) with H_2O in the feedstock. Reaction conditions: steady-state testing, [CO] = [O_2] = 1%, 5% H_2O (when used), and balanced with Ar, at WHSV of 200 000 or 300 000 mL·g_{cat}^{-1}·h^{-1}.

Figure S8 of the Supporting Information shows the EDS mapping images for 1.0Pt/CA-a and 1.0Pt/CA-HD-a. It was observed that there were no apparent changes on the morphology of the catalysts after reduction activation, and the Pt distribution was still closely associated with Ce distribution. Consistent with the observation from *in situ* DRIFTS of CO adsorption and EXAFS results, in AC-STEM images (Figure 3 and Figure S9 of the Supporting Information), Pt_C was present on both catalysts with similar size distributions but totally different interactions with CeO_2. Specifically, on 1.0Pt/CA-a, Pt_C species with an average size of *ca.* 1.8 nm were observed, primarily in the adsorbed state on the CeO_2 surface without crystal plane matching between Pt_C and CeO_2 (panels a–o of Figure 3 and Figures S9a and S10a of the Supporting Information). In clear contrast, on 1.0Pt/CA-HD-a, Pt_C species with an average size of *ca.* 1.7 nm and the crystal plane matching between Pt_C (111) and CeO_2 (020) were clearly observed (panels p–x of Figure 3 and Figures S9b and S10b of the Supporting Information), with the bottom layer of Pt atoms embedded in the CeO_2 surface matrix. Such a unique Pt_C structure embedded in the CeO_2 surface matrix, which originated from the reduction activation of Pt_1 species on CA-HD with an enhanced Pt–CeO_2 interaction, could be responsible for the superior CO oxidation activity of the 1.0Pt/CA-HD-a catalyst. In our previous study, we concluded that the CeO_2 surface-embedded Pt single-layer structure could more effectively activate the oxygen species at the Pt–CeO_2 interface than the CeO_2 surface-adsorbed Pt single-layer structure,[40] and this phenomenon should also be applicable to the case of multilayer Pt_C in this study, which can be verified in the following characterization sections.

As summarized in Figure 4a, the surface defects of the CA support could be significantly increased by H_2 reduction treatment, leading to the exclusive formation of Pt_1 species on the Pt/CA-HD catalyst with Pt_1 embedded in the CeO_2 surface matrix substituting the Ce site, in clear contrast to the mixture state of Pt_1 and Pt_C species on regular Pt/CA without defect enrichment. Reduction activation was confirmed to be an effective way to transform the less active Pt_1 species into more active Pt_C species on both catalysts. The unique Pt_C structures with the bottom layer of Pt atoms embedded in the CeO_2 surface matrix could be formed after the reduction activation of Pt/CA-HD, while only randomly adsorbed Pt_C structures could be formed on activated Pt/CA. Considering that the 1.0Pt/CA-HD-a catalyst showed much higher activity and a similar Pt cluster size compared to 1.0Pt/CA-a, it can be concluded that the bottom-layer-embedded Pt_C structures in the CeO_2 lattice matrix were more active for the CO oxidation reaction than the adsorbed Pt_C structures on the CeO_2 surface.

3.4. Catalytic Stability. The catalytic stability of the 1.0Pt/CA and 1.0Pt/CA-HD catalysts before and after reduction activation was measured at temperatures up to 500 °C for CO oxidation (Figure 4b). It was observed that there was no apparent change in the CO oxidation activity for both 1.0Pt/CA and 1.0Pt/CA-HD catalysts during the cycling test, suggesting that the Pt sites in these two as-prepared catalysts were stable under the reaction conditions. On 1.0Pt/CA-a and 1.0Pt/CA-HD-a catalysts, the CO oxidation activity only slightly declined after the first run and then remained stable during the following test cycles. Notably, the 1.0Pt/CA-HD-a catalyst consistently showed much higher CO oxidation activity than the 1.0Pt/CA-a catalyst, with the stabilized T50 at 118 °C on 1.0Pt/CA-HD-a compared to that at 145 °C on 1.0Pt/CA-a. With the presence of H_2O in the reaction flow, significant improvement of CO oxidation activity was observed on both 1.0Pt/CA-a and 1.0Pt/CA-HD-a catalysts (Figure 4c and Figure S11 of the Supporting Information), which was in line with the observation that H_2O has a positive effect on CO oxidation over Pt-CeO_2 based catalysts.[8,41,42] It is noteworthy that the 1.0Pt/CA-HD-a catalyst always outperformed the 1.0Pt/CA-a catalyst under the wet reaction conditions, at either the fixed reaction temperature (Figure 4c) or the varied reaction temperatures (Figure S11 of the Supporting Information). These results confirmed that the Pt/CA catalysts were catalytically stable and exhibited excellent H_2O tolerance,

https://doi.org/10.1021/acs.est.4c03078
Environ. Sci. Technol. 2024, 58, 12731–12741

with the 1.0Pt/CA-HD-a catalyst performing the best. The CO oxidation rate and turnover frequency (TOF) on 1.0Pt/CA-HD-a were further calculated and compared to other Pt-CeO_2-based catalysts reported in the literature. As listed in Table S3 of the Supporting Information, at 125 °C, the reaction rate (418 mmol·g_{Pt}^{-1}·s^{-1}) and TOF (0.601 s^{-1}) on 1.0Pt/CA-HD-a surpassed those on most Pt-CeO_2-based catalysts, showing high potential for practical applications.

3.5. Crystal Structure and Surface Elemental Composition. As shown in Figure S12 of the Supporting Information, all 1.0Pt/CA and 1.0Pt/CA-HD catalysts exhibited similar crystal structures, containing a mixture of γ-Al_2O_3 and cubic fluorite CeO_2, before and after reduction activation. No Pt species was detected in these catalysts, which should be due to the low Pt loading and relatively high Pt dispersion. The crystallite sizes of CeO_2 were calculated using the Scherrer equation and were found to be smaller in the 1.0Pt/CA-HD (9.5 nm) and 1.0Pt/CA-HD-a (6.7 nm) catalysts compared to those in the 1.0Pt/CA (10.3 nm) and 1.0Pt/CA-a (7.6 nm) catalysts, respectively, as inserted in Figure S12 of the Supporting Information. In addition, it is interesting to see that the reduction activation led to a significant decrease of the CeO_2 crystallite size in 1.0Pt/CA-a and 1.0Pt/CA-HD-a catalysts compared to their unreduced 1.0Pt/CA and 1.0Pt/CA-HD precursor catalysts, respectively, possibly as a result of the disruption of the long-range order of CeO_2 and the formation of rich Ce^{3+} species in the activation process. The Ce 3d XPS results, as depicted in Figure S13 of the Supporting Information, revealed the presence of both surface Ce^{3+} and Ce^{4+} species in all of the 1.0Pt/CA and 1.0Pt/CA-HD catalysts before and after activation. As expected, the 1.0Pt/CA-a and 1.0Pt/CA-HD-a catalysts indeed exhibited much higher concentrations of surface Ce^{3+} species (Figure S13 and Table S1 of the Supporting Information) compared to those of their precursor catalysts before activation. Previous work reported that the formation of richer Ce^{3+} species was usually associated with the generation of more oxygen defects on the CeO_2 surface, which was beneficial for O_2 activation.[30] The slightly higher concentration of surface Ce^{3+} species observed on 1.0Pt/CA-HD-a than on 1.0Pt/CA-a could have contributed to the higher CO oxidation activity achieved on 1.0Pt/CA-HD-a.

3.6. Structure−Activity Relationship for CO Oxidation. The reaction orders for CO and O_2 in CO oxidation were determined on all catalysts before and after activation, and the results are shown in panels a and b of Figure 5. For CO oxidation on 1.0Pt/CA, 1.0Pt/CA-a, 1.0Pt/CA-HD, and 1.0Pt/CA-HD-a, the CO reaction orders were determined as 0.20, 0.20, 1.49, and 0.11, respectively, while the O_2 reaction orders were determined as 0.30, 0.31, 0.56, and 0.19, respectively. The high CO reaction order on the 1.0Pt/CA-HD catalyst could be explained by the difficult CO adsorption on embedded Pt_1 sites without oxygen vacancies nearby, as already evidenced in our previous work.[40] On other catalysts with Pt_C sites, CO could be easily adsorbed and involved in CO oxidation, resulting in low CO reaction orders ($\leq$ 0.20). The lowest CO reaction order achieved on the 1.0Pt/CA-HD-a catalyst suggests that the embedded Pt_C sites were more beneficial for CO adsorption than adsorbed Pt_C and Pt_1 sites. The O_2 reaction orders showed a sequence similar to that of the CO reaction orders on all catalysts, decreasing in the sequence of 1.0Pt/CA-HD (0.56) > 1.0Pt/CA-a (0.31) ≈ 1.0Pt/CA (0.30) > 1.0Pt/CA-HD-a (0.19). On 1.0Pt/CA-HD-a, the lowest O_2 order for CO oxidation could be achieved, suggesting that the embedded Pt_C sites favored the O_2 adsorption/activation compared to the adsorbed Pt_C and Pt_1 sites. In summary, the embedded Pt_C sites could better facilitate both CO adsorption and O_2 adsorption/activation, contributing to the superior CO oxidation activity of the 1.0Pt/CA-HD-a catalyst. It should be noted that the similar CO and O_2 reaction orders obtained on 1.0Pt/CA-a and 1.0Pt/CA were due to the presence of adsorbed Pt_C sites in both catalysts, and the higher CO oxidation activity achieved on 1.0Pt/CA-a was mainly due to its higher density of Pt_C sites.

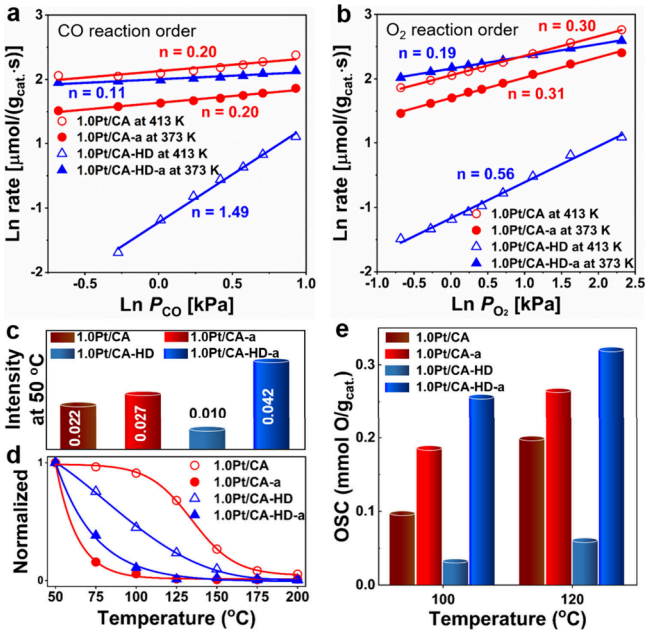

Figure 5. Kinetic study results: (a) CO reaction orders and (b) O_2 reaction orders in CO oxidation, (c) intensity for CO adsorption detected by DRIFTS at 50 °C and (d) normalized intensity for CO adsorption at different temperatures, and (e) OSC of 1.0Pt/CA, 1.0Pt/CA-a, 1.0Pt/CA-HD, and 1.0Pt/CA-HD-a catalysts at 100 and 120 °C. The kinetic study experiments were conducted under the CO conversions below 16% and the WHSV of 500 000 mL·g_{cat}^{-1}·h^{-1}. The intensity for CO adsorption was referring to the main CO adsorption peak detected by *in situ* DRIFTS experiments, and the normalized intensity for CO adsorption at different temperatures was determined by dividing the corresponding CO adsorption intensity at 50 °C.

To further investigate the CO adsorption capability of different Pt structures, *in situ* DRIFTS experiments of CO adsorption (at 25 °C)−desorption (from 50 to 200 °C) were conducted on all catalysts before and after reduction activation (panels c and d of Figure 5 and Figure S14 of the Supporting Information). At 50 °C, the CO adsorption intensity on all catalysts (Figure 5c) increased in the following order: 1.0Pt/CA-HD (0.010) < 1.0Pt/CA (0.022) < 1.0Pt/CA-a (0.027) < 1.0Pt/CA-HD-a (0.042). This trend was in accordance with the kinetic study results (CO reaction order), confirming again that the 1.0Pt/CA-HD-a catalyst with embedded Pt_C sites showed higher CO adsorption capacity, while the CO adsorption on the 1.0Pt/CA-HD catalyst with embedded Pt_1 sites was rather difficult. Furthermore, the higher CO adsorption capacity on the 1.0Pt/CA-a catalyst than 1.0Pt/CA was mainly attributed to the presence of more adsorbed Pt_C sites in the former catalyst. As shown in Figure S14 of the Supporting Information, the CO adsorption intensity on all

https://doi.org/10.1021/acs.est.4c03078
Environ. Sci. Technol. 2024, 58, 12731−12741

catalysts decreased monotonically with the increased temperature. The normalized CO adsorption intensities (on the basis of the corresponding reference CO intensity at 50 °C) as a function of the desorption temperature are shown in Figure 5d, to reveal the CO desorption rates on different catalysts. It can be clearly seen that the decline degree of CO adsorption intensity followed the order of 1.0Pt/CA-*a* > 1.0Pt/CA-HD-*a* > 1.0Pt/CA-HD > 1.0Pt/CA. In combination with the CO oxidation activity, these results suggest that the amount of Pt sites for CO adsorption was more critical than the strength of CO−Pt bonding for the CO oxidation on different catalysts. To further investigate the O_2 activation and oxygen mobility within all catalysts, the dynamic OSC was determined by CO/O_2 pulse cycling experiments for 1.0Pt/CA and 1.0Pt/CA-HD catalysts before and after activation (Figure 5e). It can be observed that the OSC values for all catalysts followed the sequence of 1.0Pt/CA-HD < 1.0Pt/CA < 1.0Pt/CA-a < 1.0Pt/CA-HD-a at different temperatures. Consistent with the kinetic study results (O_2 reaction order), the 1.0Pt/CA-HD-a catalyst with embedded Pt_C sites indeed exhibited superior O_2 activation ability. To better reveal the relationship between the CO adsorption capacity, OSC function, and CO oxidation activity on these catalysts, the plots of the CO adsorption intensity and OSC values versus T50 for the CO oxidation light-off are presented in Figure 6. It was evident that the CO oxidation activity on Pt-CeO_2-Al_2O_3 serial catalysts was strongly correlated to the Pt sites with distinct CO adsorption capacity and an O_2 activation ability. The 1.0Pt/CA-HD-a catalyst with embedded Pt_C sites showed significantly enhanced CO adsorption and promoted O_2 activation, thus contributing to its superior CO oxidation activity at low temperatures.

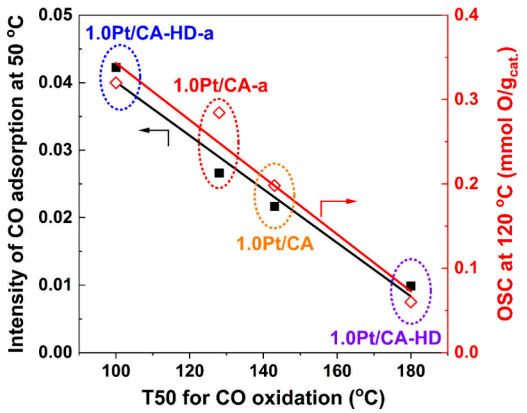

Figure 6. Correlation between the T50 for the CO oxidation reaction and the intensity of CO adsorption at 50 °C as well as the OSC values measured at 120 °C on all Pt/CA catalysts.

To clarify the role of Pt active sites in CO oxidation, *in situ* XANES analysis of the Pt L_3-edge in 1.0Pt/CA-a and 1.0Pt/CA-HD-a catalysts was conducted under different testing conditions. As shown in Figure 7 and Figure S15 of the Supporting Information, a consistent trend in the changes of white line intensities of Pt L_3-edge XANES and, accordingly, the average Pt oxidation states was observed on both catalysts from experimental steps 1−4. In the reaction flow (CO + O_2), with the temperature increasing from 25 to 100 °C, both catalysts exhibited a decline in the Pt oxidation state, indicating the partial reduction of PtO_x clusters by CO during the reaction. Upon the change from a CO + O_2 flow to a CO flow at 100 °C, a further decrease in the Pt oxidation state occurred as a result of a further reduction of PtO_x clusters. Interestingly, when the reaction flow was switched back to the reaction flow (CO + O_2) at 100 °C, there was no substantial change in the Pt oxidation state on both catalysts. These results suggest that the partially reduced Pt species remained stable and showed high resistance to reoxidation by O_2, underscoring the crucial role of partially reduced Pt species in the CO adsorption and activation, while the O_2 activation should not take place on the Pt surface (but at the Pt_C−CeO_2 interface). In comparison of the Pt oxidation state in 1.0Pt/CA-HD-a to that in 1.0Pt/CA-a under different testing conditions, a consistently higher Pt oxidation state was observed in the former catalyst. These results suggest that the stronger interaction between Pt_C and CeO_2 in the 1.0Pt/CA-HD-a catalyst remained constantly stable under different conditions and could effectively facilitate the oxygen mobility at the Pt_C−CeO_2 interface. Therefore, the 1.0Pt/CA-HD-a catalyst showed both significantly enhanced CO adsorption and promoted O_2 activation, on which the abundant CO species adsorbed on embedded Pt_C sites could readily react with facilely mobile O from CeO_2 at the interfaces, thus exhibiting excellent low-temperature CO oxidation performance.

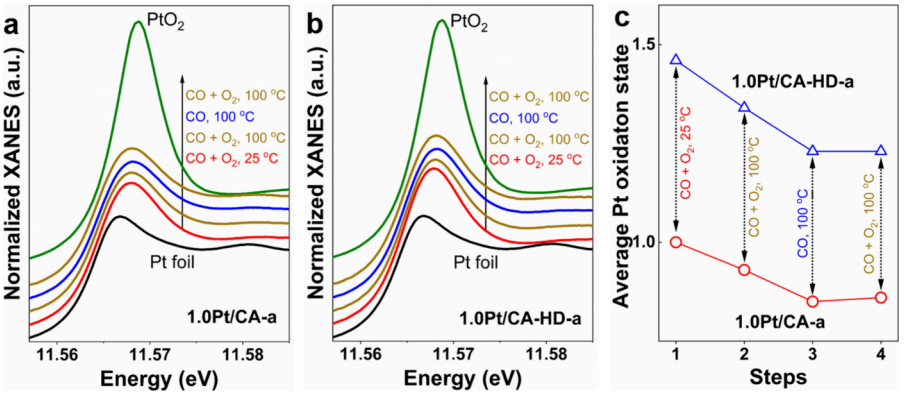

Figure 7. *In situ* XANES of Pt L_3-edge in (a) 1.0Pt/CA-a and (b) 1.0Pt/CA-HD-a catalysts and their corresponding (c) average Pt oxidation states under different testing conditions. The average Pt oxidation states were determined by the linear combination fitting of Pt L_3-edge XANES using Pt foil and PtO_2 as references.

https://doi.org/10.1021/acs.est.4c03078
Environ. Sci. Technol. 2024, 58, 12731−12741

4. ENVIRONMENTAL IMPLICATION

CO gas emitted from diverse sources, including vehicle exhaust and industrial activities, poses significant risks to both the environment and human health. There is a continuous demand for the development of highly efficient catalysts to mitigate CO emissions at low temperatures. Precious metal catalysts, such as Pt-CeO_2, have shown great promise, although further improvement in the low-temperature activity is still needed. In this work, a universal defect enrichment strategy involving reduction pretreatment was developed for CeO_2-based supports, including CeO_2, $CeZrO_x$, and CeO_2/Al_2O_3 (CA). On these defect-enriched supports, Pt catalysts showed improved Pt dispersion and enhanced low-temperature CO oxidation activity upon reduction activation. Specifically, using the CeO_2/Al_2O_3 support with enriched surface defects (CA-HD), embedded Pt clusters (Pt_C) with the bottom layer of Pt atoms substituting the Ce cations were generated within the 1.0Pt/CA-HD-a catalyst after reduction activation (where -a is activated). These embedded Pt_C sites exhibited superior catalytic activity in CO oxidation in comparison to the adsorbed Pt_C sites on CeO_2 within the 1.0Pt/CA-a catalyst, although they were showing similar cluster sizes. In-depth characterizations and mechanism studies suggested that the uniquely embedded Pt_C sites had a stronger interaction with CeO_2, which not only benefited the CO adsorption on Pt_C sites but also improved the O_2 activation and interfacial oxygen mobility on CeO_2. Collectively, the significantly enhanced low-temperature CO oxidation at the interfaces between Pt_C and CeO_2 could be achieved on the 1.0Pt/CA-HD-a catalyst. This work offers valuable insights into the support defect enrichment and the synthesis of metal catalysts with improved metal dispersion and superior catalytic performance for environmental catalysis applications.

■ ASSOCIATED CONTENT

Supporting Information

The Supporting Information is available free of charge at https://pubs.acs.org/doi/10.1021/acs.est.4c03078.

Catalyst characterization, curve fitting results of Pt L_3-edge EXAFS, surface atomic concentrations and Pt average oxidation states, CO oxidation activity on 1.0Pt/CeO_2-HD, 1.0Pt/$CeZrO_x$-HD, and *x*Pt/CA-HD catalysts, linear combination fitting results of Pt L_3-edge XANES, AC-STEM and EDS mapping images, H_2-TPR profiles, XRD patterns, XPS results, and *in situ* DRIFTS study (PDF)

■ AUTHOR INFORMATION

Corresponding Author

Fudong Liu − *Department of Chemical and Environmental Engineering, University of California, Riverside, Riverside, California 92521, United States; Department of Civil, Environmental, and Construction Engineering, Catalysis Cluster for Renewable Energy and Chemical Transformations (REACT), NanoScience Technology Center (NSTC), University of Central Florida, Orlando, Florida 32816, United States;* orcid.org/0000-0001-8771-5938; Phone: 951-827-1480; Email: fudong.liu@ucr.edu

Authors

Shaohua Xie − *Department of Civil, Environmental, and Construction Engineering, Catalysis Cluster for Renewable Energy and Chemical Transformations (REACT), NanoScience Technology Center (NSTC), University of Central Florida, Orlando, Florida 32816, United States;* orcid.org/0000-0003-1550-7421

Yue Lu − *Beijing Key Laboratory of Microstructure and Properties of Solids, Faculty of Materials and Manufacturing, Beijing University of Technology, Beijing 100124, People's Republic of China;* orcid.org/0000-0001-9800-3792

Kailong Ye − *Department of Civil, Environmental, and Construction Engineering, Catalysis Cluster for Renewable Energy and Chemical Transformations (REACT), NanoScience Technology Center (NSTC), University of Central Florida, Orlando, Florida 32816, United States*

Wei Tan − *Department of Civil, Environmental, and Construction Engineering, Catalysis Cluster for Renewable Energy and Chemical Transformations (REACT), NanoScience Technology Center (NSTC), University of Central Florida, Orlando, Florida 32816, United States; State Key Laboratory of Pollution Control and Resource Reuse, School of the Environment, Jiangsu Key Laboratory of Vehicle Emissions Control, School of Chemistry and Chemical Engineering, Center of Modern Analysis, Nanjing University, Nanjing, Jiangsu 210023, People's Republic of China;* orcid.org/0000-0002-1481-9346

Sufeng Cao − *Department of Chemical and Biological Engineering, Tufts University, Medford, Massachusetts 02155, United States; Aramco Boston Research Center, Cambridge, Massachusetts 02139, United States*

Chunying Wang − *Center for Excellence in Regional Atmospheric Environment, Institute of Urban Environment, Chinese Academy of Sciences, Xiamen, Fujian 361021, People's Republic of China;* orcid.org/0009-0005-0987-4534

Daekun Kim − *Department of Civil, Environmental, and Construction Engineering, Catalysis Cluster for Renewable Energy and Chemical Transformations (REACT), NanoScience Technology Center (NSTC), University of Central Florida, Orlando, Florida 32816, United States*

Xing Zhang − *Department of Civil, Environmental, and Construction Engineering, Catalysis Cluster for Renewable Energy and Chemical Transformations (REACT), NanoScience Technology Center (NSTC), University of Central Florida, Orlando, Florida 32816, United States;* orcid.org/0009-0001-6566-1921

Jeremia Loukusa − *Department of Civil, Environmental, and Construction Engineering, Catalysis Cluster for Renewable Energy and Chemical Transformations (REACT), NanoScience Technology Center (NSTC), University of Central Florida, Orlando, Florida 32816, United States;* orcid.org/0009-0000-1636-0092

Yaobin Li − *Center for Excellence in Regional Atmospheric Environment, Institute of Urban Environment, Chinese Academy of Sciences, Xiamen, Fujian 361021, People's Republic of China;* orcid.org/0000-0002-6496-8382

Yan Zhang − *Center for Excellence in Regional Atmospheric Environment, Institute of Urban Environment, Chinese Academy of Sciences, Xiamen, Fujian 361021, People's Republic of China;* orcid.org/0000-0002-5423-8255

Lu Ma − *National Synchrotron Light Source II (NSLS-II), Brookhaven National Laboratory, Upton, New York 11973, United States*

https://doi.org/10.1021/acs.est.4c03078
Environ. Sci. Technol. 2024, 58, 12731−12741

Steven N. Ehrlich − *National Synchrotron Light Source II (NSLS-II), Brookhaven National Laboratory, Upton, New York 11973, United States*

Nebojsa S. Marinkovic − *Department of Chemical Engineering, Columbia University, New York, New York 10027, United States;* orcid.org/0000-0003-3579-3453

Jiguang Deng − *Beijing Key Laboratory for Green Catalysis and Separation, Key Laboratory of Beijing on Regional Air Pollution Control, Key Laboratory of Advanced Functional Materials, Ministry of Education of China, Faculty of Environment and Life, Beijing University of Technology, Beijing 100124, People's Republic of China;* orcid.org/0000-0001-7768-3688

Maria Flytzani-Stephanopoulos − *Department of Chemical and Biological Engineering, Tufts University, Medford, Massachusetts 02155, United States*

Complete contact information is available at: https://pubs.acs.org/10.1021/acs.est.4c03078

Notes

The authors declare no competing financial interest.

▲Maria Flytzani-Stephanopoulos passed away on October 28, 2019.

■ ACKNOWLEDGMENTS

Fudong Liu acknowledges the National Science Foundation (Grant CHE-1955343) and Startup Fund from the University of California, Riverside (UCR). Shaohua Xie, Daekun Kim, and Xing Zhang thank the support from the Preeminent Postdoctoral Program (P3) at the University of Central Florida (UCF). Fudong Liu sincerely thanks Dr. Marcos Schöneborn at Sasol for providing raw materials in catalyst synthesis and Prof. Laurene Tetard for providing resources in Raman spectra measurement. This research used beamline 7-BM (QAS) of the National Synchrotron Light Source II, a U.S. Department of Energy (DOE) Office of Science User Facility operated for the U.S. DOE Office of Science by Brookhaven National Laboratory under Contract DE-SC0012704. Beamline operations were supported in part by the Synchrotron Catalysis Consortium (U.S. DOE Office of Basic Energy Sciences, Grant DE-SC0012335).

■ REFERENCES

(1) Li, X.; Huang, Y.; Liu, B. Catalyst: Single-atom catalysis: Directing the way toward the nature of catalysis. *Chem* **2019**, *5* (11), 2733−2735.

(2) Kaiser, S. K.; Chen, Z.; Faust Akl, D.; Mitchell, S.; Perez-Ramirez, J. Single-atom catalysts across the periodic table. *Chem. Rev.* **2020**, *120* (21), 11703−11809.

(3) Liu, D.; He, Q.; Ding, S.; Song, L. Structural regulation and support coupling effect of single-atom catalysts for heterogeneous catalysis. *Adv. Energy Mater.* **2020**, *10* (32), 2001482.

(4) Resasco, J.; Christopher, P. Atomically dispersed Pt-group catalysts: Reactivity, uniformity, structural evolution, and paths to increased functionality. *J. Phys. Chem. Lett.* **2020**, *11* (23), 10114−10123.

(5) Xue, Z.; Yan, M.; Zhang, Y.; Xu, J.; Gao, X.; Wu, Y. Understanding the injection process of hydrogen on Pt_1-TiO_2 surface for photocatalytic hydrogen evolution. *Appl. Catal., B* **2023**, *325*, 122303.

(6) Zhu, M.; Zhao, C.; Liu, X.; Wang, X.; Zhou, F.; Wang, J.; Hu, Y.; Zhao, Y.; Yao, T.; Yang, L. M.; Wu, Y. Single atomic cerium sites with a high coordination number for efficient oxygen reduction in proton-exchange membrane fuel cells. *ACS Catal.* **2021**, *11* (7), 3923−3929.

(7) Zhang, N.; Ye, C.; Yan, H.; Li, L.; He, H.; Wang, D.; Li, Y. Single-atom site catalysts for environmental catalysis. *Nano Res.* **2020**, *13* (12), 3165−3182.

(8) Wang, H.; Liu, J.-X.; Allard, L. F.; Lee, S.; Liu, J.; Li, H.; Wang, J.; Wang, J.; Oh, S. H.; Li, W.; Flytzani-Stephanopoulos, M.; Shen, M.; Goldsmith, B. R.; Yang, M. Surpassing the single-atom catalytic activity limit through paired Pt-O-Pt ensemble built from isolated Pt_1 atoms. *Nat. Commun.* **2019**, *10* (1), 3808.

(9) Ding, K.; Gulec, A.; Johnson, A. M.; Schweitzer, N. M.; Stucky, G. D.; Marks, L. D.; Stair, P. C. Identification of active sites in CO oxidation and water-gas shift over supported Pt catalysts. *Science* **2015**, *350*, 189−192.

(10) Nie, L.; Mei, D. H.; Xiong, H. F.; Peng, B.; Ren, Z. B.; Hernandez, X. I. P.; DeLaRiva, A.; Wang, M.; Engelhard, M. H.; Kovarik, L.; Datye, A. K.; Wang, Y. Activation of surface lattice oxygen in single-atom Pt/CeO_2 for low-temperature CO oxidation. *Science* **2017**, *358* (6369), 1419−1423.

(11) Lu, Y.; Zhou, S.; Kuo, C.-T.; Kunwar, D.; Thompson, C.; Hoffman, A. S.; Boubnov, A.; Lin, S.; Datye, A. K.; Guo, H.; Karim, A. M. Unraveling the intermediate reaction complexes and critical role of support-derived oxygen atoms in CO oxidation on single-atom Pt/CeO_2. *ACS Catal.* **2021**, *11* (14), 8701−8715.

(12) Jeong, H.; Shin, D.; Kim, B. S.; Bae, J.; Shin, S.; Choe, C.; Han, J. W.; Lee, H. Controlling the oxidation dtate of Pt dingle stoms for maximizing catalytic activity. *Angew. Chem., Int. Ed.* **2020**, *59* (46), 20691−20696.

(13) Jiang, D.; Yao, Y.; Li, T.; Wan, G.; Pereira-Hernandez, X. I.; Lu, Y.; Tian, J.; Khivantsev, K.; Engelhard, M. H.; Sun, C.; Garcia-Vargas, C. E.; Hoffman, A. S.; Bare, S. R.; Datye, A. K.; Hu, L.; Wang, Y. Tailoring the local environment of platinum in single-atom Pt_1/CeO_2 catalysts for robust low-temperature CO oxidation. *Angew. Chem., Int. Ed.* **2021**, *60* (50), 26054−26062.

(14) Tang, Y.; Wang, Y. G.; Li, J. Theoretical investigations of Pt_1@CeO_2 single-atom catalyst for CO oxidation. *J. Phys. Chem. C* **2017**, *121* (21), 11281−11289.

(15) Pereira-Hernández, X. I.; DeLaRiva, A.; Muravev, V.; Kunwar, D.; Xiong, H.; Sudduth, B.; Engelhard, M.; Kovarik, L.; Hensen, E. J. M.; Wang, Y.; Datye, A. K. Tuning Pt-CeO_2 interactions by high-temperature vapor-phase synthesis for improved reducibility of lattice oxygen. *Nat. Commun.* **2019**, *10* (1), 1358.

(16) Xie, S.; Tan, W.; Wang, C.; Arandiyan, H.; Garbrecht, M.; Ma, L.; Ehrlich, S. N.; Xu, P.; Li, Y.; Zhang, Y.; Collier, S.; Deng, J.; Liu, F. Structure-activity relationship of Pt catalyst on engineered ceria-alumina support for CO oxidation. *J. Catal.* **2022**, *405*, 236−248.

(17) Xie, S.; Wang, Z.; Tan, W.; Zhu, Y.; Collier, S.; Ma, L.; Ehrlich, S. N.; Xu, P.; Yan, Y.; Xu, T.; Deng, J.; Liu, F. Highly active and stable palladium catalysts on novel ceria-alumina supports for efficient oxidation of carbon monoxide and hydrocarbons. *Environ. Sci. Technol.* **2021**, *55* (11), 7624−7633.

(18) Dvořák, F.; Farnesi Camellone, M.; Tovt, A.; Tran, N. D.; Negreiros, F. R.; Vorokhta, M.; Skála, T.; Matolinová, I.; Mysliveček, J.; Matolín, V.; Fabris, S. Creating single-atom Pt-ceria catalysts by surface step decoration. *Nat. Commun.* **2016**, *7*, 10801.

(19) Li, X.; Pereira-Hernandez, X. I.; Chen, Y.; Xu, J.; Zhao, J.; Pao, C. W.; Fang, C. Y.; Zeng, J.; Wang, Y.; Gates, B. C.; Liu, J. Functional CeO_x nanoglues for robust atomically dispersed catalysts. *Nature* **2022**, *611* (7935), 284−288.

(20) Farrauto, R. J.; Deeba, M.; Alerasool, S. Gasoline automobile catalysis and its historical journey to cleaner air. *Nat. Catal.* **2019**, *2* (7), 603−613.

(21) Lu, Y.; Zhang, Z.; Lin, F.; Wang, H.; Wang, Y. Single-atom Automobile Exhaust Catalysts. *ChemNanoMat* **2020**, *6* (12), 1659−1682.

(22) Boronin, A. I.; Slavinskaya, E. M.; Figueroba, A.; Stadnichenko, A. I.; Kardash, T. Y.; Stonkus, O. A.; Fedorova, E. A.; Muravev, V. V.; Svetlichnyi, V. A.; Bruix, A.; Neyman, K. M. CO oxidation activity of Pt/CeO_2 catalysts below 0 °C: Platinum loading effects. *Appl. Catal., B* **2021**, *286*, 119931.

(23) Yang, C.; Lu, Y.; Zhang, L.; Kong, Z.; Yang, T.; Tao, L.; Zou, Y.; Wang, S. Defect engineering on CeO_2-based catalysts for heterogeneous catalytic applications. *Small Struct.* **2021**, *2* (12), 2100058.
(24) Huang, B.; Gillen, R.; Robertson, J. Study of CeO_2 and its native defects by density functional theory with repulsive potential. *J. Phys. Chem. C* **2014**, *118* (42), 24248−24256.
(25) Zhang, S.; Huang, Z.-Q.; Ma, Y.; Gao, W.; Li, J.; Cao, F.; Li, L.; Chang, C.-R.; Qu, Y. Solid frustrated-Lewis-pair catalysts constructed by regulations on surface defects of porous nanorods of CeO_2. *Nat. Commun.* **2017**, *8*, 15266.
(26) Lee, W.; Chen, S. Y.; Chen, Y. S.; Dong, C. L.; Lin, H. J.; Chen, C. T.; Gloter, A. Defect structure guided room temperature ferromagnetism of Y-doped CeO_2 nanoparticles. *J. Phys. Chem. C* **2014**, *118* (45), 26359−26367.
(27) Choudhury, B.; Choudhury, A. Lattice distortion and corresponding changes in optical properties of CeO_2 nanoparticles on Nd doping. *Curr. Appl. Phys.* **2013**, *13* (1), 217−223.
(28) Soni, S.; Kumar, S.; Dalela, B.; Kumar, S.; Alvi, P. A.; Dalela, S. Defects and oxygen vacancies tailored structural and optical properties in CeO_2 nanoparticles doped with Sm^{3+} cation. *J. Alloys Compd.* **2018**, *752*, 520−531.
(29) Yuejuan, W.; Jingmeng, M.; Mengfei, L.; Ping, F.; Mai, H. Preparation of high-surface area nano-CeO_2 by template-assisted precipitation method. *J. Rare Earths* **2007**, *25* (1), 58−62.
(30) Schilling, C.; Hofmann, A.; Hess, C.; Ganduglia-Pirovano, M. V. Raman spectra of polycrystalline CeO_2: A density functional theory study. *J. Phys. Chem. C* **2017**, *121* (38), 20834−20849.
(31) Daniel, M.; Loridant, S. Probing reoxidation sites byin situRaman spectroscopy: Differences between reduced CeO_2 and Pt/CeO_2. *J. Raman Spectrosc.* **2012**, *43* (9), 1312−1319.
(32) Zhang, S.; Li, X. S.; Chen, B.; Zhu, X.; Shi, C.; Zhu, A. M. CO oxidation activity at room temperature over Au/CeO_2 catalysts: Disclosure of induction period and humidity effect. *ACS Catal.* **2014**, *4* (10), 3481−3489.
(33) Wu, Z.; Li, M.; Mullins, D. R.; Overbury, S. H. Probing the surface sites of CeO_2 nanocrystals with well-defined surface planes via methanol adsorption and desorption. *ACS Catal.* **2012**, *2* (11), 2224−2234.
(34) Bazin, P.; Saur, O.; Lavalley, J. C.; Daturi, M.; Blanchard, G. FT-IR study of CO adsorption on Pt/CeO_2: Characterisation and structural rearrangement of small Pt particles. *Phys. Chem. Chem. Phys.* **2005**, *7* (1), 187−194.
(35) Bera, P.; Priolkar, K. R.; Gayen, A.; Sarode, P. R.; Hegde, M. S.; Emura, S.; Kumashiro, R.; Jayaram, V.; Subbanna, G. N. Ionic dispersion of Pt over CeO_2 by the combustion method: Structural investigation by XRD, TEM, XPS, and EXAFS. *Chem. Mater.* **2003**, *15*, 2049−2060.
(36) Derevyannikova, E. A.; Kardash, T. Y.; Stadnichenko, A. I.; Stonkus, O. A.; Slavinskaya, E. M.; Svetlichnyi, V. A.; Boronin, A. I. Structural insight into strong Pt-CeO_2 interaction: From single Pt atoms to PtO_x clusters. *J. Phys. Chem. C* **2019**, *123* (2), 1320−1334.
(37) Ke, J.; Zhu, W.; Jiang, Y.; Si, R.; Wang, Y. J.; Li, S. C.; Jin, C.; Liu, H.; Song, W. G.; Yan, C. H.; Zhang, Y. W. Strong local coordination structure effects on subnanometer PtO_x clusters over CeO_2 nanowires probed by low-temperature CO oxidation. *ACS Catal.* **2015**, *5* (9), 5164−5173.
(38) Avanesian, T.; Dai, S.; Kale, M. J.; Graham, G. W.; Pan, X.; Christopher, P. Quantitative and atomic-scale view of CO-induced Pt nanoparticle surface reconstruction at saturation coverage via DFT calculations coupled with *in situ* TEM and IR. *J. Am. Chem. Soc.* **2017**, *139* (12), 4551−4558.
(39) Meunier, F. C. Relevance of IR spectroscopy of adsorbed CO for the characterization of heterogeneous catalysts containing isolated atoms. *J. Phys. Chem. C* **2021**, *125* (40), 21810−21823.
(40) Xie, S.; Liu, L.; Lu, Y.; Wang, C.; Cao, S.; Diao, W.; Deng, J.; Tan, W.; Ma, L.; Ehrlich, S. N.; Li, Y.; Zhang, Y.; Ye, K.; Xin, H.; Flytzani-Stephanopoulos, M.; Liu, F. Pt atomic single-layer catalyst embedded in defect-enriched ceria for efficient CO oxidation. *J. Am. Chem. Soc.* **2022**, *144* (46), 21255−21266.
(41) Wang, C.; Gu, X.-K.; Yan, H.; Lin, Y.; Li, J.; Liu, D.; Li, W.-X.; Lu, J. Water-mediated Mars−Van Krevelen mechanism for CO oxidation on ceria-supported single-atom Pt_1 catalyst. *ACS Catal.* **2017**, *7* (1), 887−891.
(42) Wang, Y.; Ma, J.; Wang, X.; Zhang, Z.; Zhao, J.; Yan, J.; Du, Y.; Zhang, H.; Ma, D. Complete CO oxidation by O_2 and H_2O over Pt−$CeO_{2-\delta}$/MgO following Langmuir−Hinshelwood and Mars−van Krevelen mechanisms, respectively. *ACS Catal.* **2021**, *11* (19), 11820−11830.

https://doi.org/10.1021/acs.est.4c03078
Environ. Sci. Technol. 2024, 58, 12731−12741